Prepared for submission to JCAP

NSF-KITP-13-128
IFIC/13-48

Impact of nucleon matrix element uncertainties on the interpretation of direct and indirect dark matter search results

R. Ruiz de Austri[1,3] **C. Pérez de los Heros**[2,3]

[1]Instituto de Física Corpuscular, IFIC-UV/CSIC, Valencia, Spain
[2]Department of Physics and Astronomy, Uppsala University. Uppsala, Sweden
[3]Kavli Institute for Theoretical Physics, University of California, Santa Barbara, USA

E-mail: rruiz@ific.uv.es, cph@physics.uu.se

Abstract. We study in detail the impact of the current uncertainty in nucleon matrix elements on the sensitivity of direct and indirect experimental techniques for dark matter detection. We perform two scans in the framework of the cMSSM: one using recent values of the pion-sigma term obtained from Lattice QCD, and the other using values derived from experimental measurements. The two choices correspond to extreme values quoted in the literature and reflect the current tension between different ways of obtaining information about the structure of the nucleon. All other inputs in the scans, astrophysical and from particle physics, are kept unchanged. We use two experiments, XENON100 and IceCube, as benchmark cases to illustrate our case. We find that the interpretation of dark matter search results from direct detection experiments is more sensitive to the choice of the central values of the hadronic inputs than the results of indirect search experiments. The allowed regions of cMSSM parameter space after including XENON100 constraints strongly differ depending on the assumptions on the hadronic matrix elements used. On the other hand, the constraining potential of IceCube is almost independent of the choice of these values.

Keywords: nuclear form factors, strangeness content of the nucleon, dark matter, neutrino telescopes

Contents

1 Introduction

The search for dark matter is one of the most active fields in particle and astroparticle physics today. Generic candidates that can account for the cold dark matter required to fit cosmological observations must be stable, massive and weakly interacting with normal matter, and they are usually referred to as WIMPs (weakly interacting massive particles). There are various theoretical possibilities providing viable candidates for dark matter. Natural choices arise in extensions of the Standard Model of particle physics, where new particles are introduced which have the right lifetime and annihilation cross section to have survived as thermal relics from the early universe. In particular, stable particles predicted in different flavors of the Minimal Supersymmetric extension to the Standard Model (MSSM) have been extensively studied as dark matter candidates, all having in common that they have weak-type cross sections with ordinary matter. A good dark matter relic particle is the lightest neutralino, which is the mass eigenstate of a mixture of bino, wino (the superpartners of the B, W^0 gauge bosons) and higgsinos (the superpartners of the H_1^0, H_2^0 Higgs bosons). In a wide class of models, the neutralino is the lightest stable supersymmetric particle.

A realistic interpretation of the results of dark matter searches must include not only the systematic uncertainties of the experiments themselves, but also uncertainties in the ingredients which enter in the calculation of expected signals. These include uncertainties in astrophysical inputs as well as in nuclear physics inputs. Recent parameter scans of different supersymmetric scenarios, including the present work, include uncertainties in the estimation of the local dark matter density and velocity dispersion, as well as in nuclear physics quantities, like in the hadronic nucleon matrix elements [1–5]. However, it was already pointed out in 1996 by the authors in [6] that "the uncertainty in the pion-nucleon sigma term is perhaps the largest source of uncertainty" in the calculation of the WIMP-nucleon cross section, and therefore on the interpretation of the results from dark matter search experiments. The authors of [7–9] have also brought up the issue of the quark content of the nucleon in the context of the WIMP-nucleon cross section, specifically on the strange-quark component.

Indeed the capture of WIMPs in celestial bodies and their scattering off target nuclei in direct detection experiments, depend on the WIMP-nucleus cross section, the results from both techniques being complementary [10]. But the calculation of the WIMP-nucleus cross section from the fundamental interactions of WIMPs with quarks and gluons involves two further layers of complexity: the parametrization of the nucleon structure in terms of quark and gluon structure functions and the description of a nuclear state as a coherent superposition of nucleons [11]. Already the first step presents experimental challenges since the structure of nucleons at low momentum transfer is difficult to directly probe experimentally, specially the strangeness content. Recent progress from Lattice QCD in combination with chiral effective field theory, has improved considerably the uncertainties in the calculations of the hadron masses and the light quark and strange quark sigma terms [12, 13]. But there is still some tension with the central values obtained from experimental results. The second step, the description of a nucleus as a system of nucleons, is relevant when considering different target nuclei for capture or scattering, where the uncertainties in the nuclear from factors can play an important role in the calculations of the total WIMP-nucleus cross section. A recent analysis in the case of direct searches can be found in [14].

In this paper we focus on the effect of using different estimations of the strangeness component of the nucleon on the interpretation of signal rates in neutrino telescopes, and its correlation with the results from direct search experiments.

We extend the method developed in [15] and we work in the context of the Constrained Minimal Supersymmetric Extension of the Standard Model (cMSSM) [16]. We will assume that the lightest neutralino is the dark matter candidate. We use the effective area and angular resolution of IceCube in its 86-string configuration to make concrete predictions on the effect on the cMSSM, based on their null result on dark matter search from the Sun, but the conclusions can easily be extended to any generic neutrino telescope. For direct searches we use the most recent XENON100 results. Keeping all other inputs unchanged, we perform scans over the cMSSM parameter space using different values for the hadronic variables involved. In a first scan, we use the value of the pion-nucleon sigma term, $\sigma_{\pi N}$, and the contribution of strangeness to the total proton spin from recent lattice QCD estimations. We label results from this choice as "LQCD" in the rest of the paper. In a second approach, we base our inputs for the nucleon matrix elements on experimentally obtained values of the spin content of the nucleon and of $\sigma_{\pi N}$. Given that there is a wide range of values in the literature for $\sigma_{\pi N}$, extracted from accelerator data using different methods, we chose a high value of 74$\pm$12 MeV which strongly differs from the LQCD value of 43$\pm$6.1 MeV. We cover in this way the range of values of $\sigma_{\pi N}$ quoted by different groups, and we illustrate the maximum effect that the uncertainty on the determination of this quantity can have on dark matter searches. We label results from this second choice as "Experiment" in the rest of the paper. In all cases, we compute the expected number of events in IceCube and XENON100 and evaluate the power of these experiments to constrain the cMSSM parameter space, the differences in each case being due to the different choices of inputs for the nucleon matrix elements. We note that even if we work in the framework of the cMSSM, the effect of the different choices of the matrix elements are rather decoupled from the details of the model, since they enter as a scaling factor in the calculation of the WIMP-nucleon cross section (see equations 2.1 and 2.2 below). So a generalization of our conclusions to other generic supersymmetric models is possible.

The paper is organized as follows. In section 2 we summarize the relevant components of the neutralino cross section with nucleons. In section 3 we present the theoretical and

statistical framework and provide details about the supersymmetric model we study, the nuisance parameters, the implementation of the experimental constraints as well as the scanning technique used. In section 4 we present the results from the different scans and comment on the conclusions that can be extracted for direct and indirect dark matter searches. Finally, we present our conclusions in section 5.

2 The WIMP-nucleon cross section and nucleon matrix elements

The interaction of WIMPs with a target material depends on a first instance on the total scattering cross section of the WIMP with the different nuclear species that make up the target. The WIMP-nucleus cross section can in turn be parametrized as a function of the fundamental WIMP-nucleon scattering cross section, which can be decomposed into a spin-independent and an spin-dependent part [6]. The spin-independent component, $\sigma^{SI}_{\chi N}$, is proportional to the square of the effective coupling of the neutralino to the nucleon, f_N

$$\frac{f_N}{m_N} = \sum_{q=u,d,s} f^N_{Tq} \frac{\alpha^s_q}{m_q} + \frac{2}{27} f^N_{TQ} \sum_{q=u,d,s} \frac{\alpha^s_q}{m_q}, \tag{2.1}$$

where N stands for p or n. The coefficients α^s_q refer to the neutralino-quark scalar couplings in the low-energy effective Lagrangian and are calculated for each point in our scans. The coefficients f^N_{Tq} are the nucleon matrix elements and represent the contributions of the light quarks to the mass of the nucleon. The second term corresponds to the interaction of the neutralino with the gluon scalar density in the nucleon, with $f^N_{TQ} = 1 - \sum_{q=u,d,s} f^N_{Tq}$. The matrix elements are defined as $f^N_{Tq} = \frac{m_q}{m_N} \langle N|\bar{q}q|N\rangle$ and can be calculated in Lattice QCD (LQCD), or derived experimentally from measurements of the pion-nucleon sigma term (they are essentially proportional to $\sigma_{\pi N}$ through a proportionality constant which is a function of the quark masses [9]). The pion-nucleon sigma term can be extracted from $\pi-$N scattering experiments and the results are extrapolated to zero exchange momentum using chiral perturbation theory (ChPT). Still, both the experimental measurements and the LQCD calculations of $\sigma_{\pi N}$ are plagued with difficulties and systematic uncertainties which result in quoted values in the literature between about 40 MeV and 80 MeV, with errors between 10% and 20% on these numbers. The range of these values (especially that derived for f^N_{Ts}) has an important impact on the computed spin-independent cross section, and therefore in the interpretation of the constraints from direct experiments which use spin-0 target nuclei. Lattice calculations of f^N_{Ts} tend to agree with the lower values extracted from experimental analyses. The Lattice world average gives a value of 0.043±0.011 for f^N_{Ts} [17], while one obtains $f^N_{Ts} = 0.046 \pm 0.013$ from recent data from the CHAOS spectrometer [18]. But analyses of the mass spectrum of exotic baryons [19] or a partial wave analysis of TRIUMF πN scattering data [20], provide much higher values for f^N_{Ts}, of about 0.4. We have performed scans using two extreme values of f^N_{Ts} (0.043 and 0.493) in order to illustrate the dependence of the interpretation of experimental dark matter searches on the current lack of precise knowledge of the value of f^N_{Ts}. In both cases we include the associated uncertainty on the central values as a nuisance parameter.

The spin-dependent part of the WIMP-nucleon cross section, $\sigma^{SD}_{\chi N}$, is of relevance for indirect experiments searching for dark matter accumulated in the Sun. $\sigma^{SD}_{\chi N}$ is proportional to the square of $a_p \langle S_p\rangle + a_n \langle S_n\rangle$, where $\langle S_{p/n}\rangle$ is the expectation value of the spin content

of the protons/neutrons in the nucleus, and the factors $a_{p/n}$ are defined as

$$a_N = \sum_{q=u,d,s} \frac{\alpha_q^a}{\sqrt{2}G_f} \Delta_q^N, \tag{2.2}$$

where, again, N stands for p or n. The axial-vector matrix elements Δ_q^N contain information about the quark spin content of the nucleon and are proportional to $\langle N|\bar{q}\gamma_\mu\gamma_5 q|N\rangle$. The coefficients α_q^a are the fundamental neutralino-quark axial couplings in the effective Lagrangian of the model. The factors Δ_q^N are better known than the f_{Tq}^Ns. Indeed the LQCD calculations [13] and the experimental values obtained by COMPASS [21, 22] for the Δ_u^N and Δ_d^N agree within 10% (see table 1). The COMPASS results are in agreement also with previous results from HERMES and SMC [23]. There is some tension, on the other hand, in the value of Δ_s^N obtained from LQCD and the experimental measurement. Even if Δ_s^N is an order of magnitude smaller than Δ_u^N or Δ_d^N, and its contribution is sub-dominant to the total cross section, we have performed scans using the value obtained from LQCD and from the COMPASS measurement. This covers the current range of uncertainty on Δ_s^N and allows us to evaluate its impact on the interpretation of indirect dark matter searches.

3 Theoretical and statistical framework

We work in the framework of the cMSSM, which assumes that supersymmetry is broken softly by gravity mediation [16] and the soft-parameters are universal at a high scale (M_X). Hence the model can be parametrized in terms of four free parameters: the common scalar mass, m_0, the gaugino mass $m_{1/2}$, the coefficient of the trilinear interaction A_0 plus the ratio between the vacuum expectation values of the Higgs bosons $\tan\beta$. Additionally the sign of the higgsino mass parameter, μ, needs to be fixed. The value of μ is determined from the conditions of radiative electroweak symmetry breaking. We fix sign(μ)= + 1, motivated by consistency arguments involving measurements of the anomalous muon magnetic moment.

We use Bayesian methods for doing inference of the cMSSM, the key ingredient being Bayes's theorem, namely

$$p(\mathbf{\Theta}|\mathbf{D}) = \frac{p(\mathbf{D}|\mathbf{\Theta})p(\mathbf{\Theta})}{p(\mathbf{D}}, \tag{3.1}$$

where $\mathbf{D}$ are the data and $\mathbf{\Theta}$ are the model parameters of interest. The equation reflects the fact that the posterior probability distribution function (pdf) $p(\mathbf{\Theta}|\mathbf{D})$ for the parameters is obtained from the likelihood function $p(\mathbf{D}|\mathbf{\Theta}) \equiv \mathcal{L}(\mathbf{\Theta})$ and the prior pdf $p(\mathbf{\Theta})$. The Bayesian evidence $p(\mathbf{D})$ is a normalization constant which in the case of model comparison can be ignored.

In order to study the constraints on a single parameter of interest θ_i, one considers the one-dimensional marginal posterior pdf. The marginal pdf is obtained from the full posterior distribution by integrating (marginalising) over the unwanted parameters in the n-dimensional parameter space

$$p(\theta_i|\mathbf{D}) = \int p(\mathbf{\Theta}|\mathbf{D}) d\theta_1 ... d\theta_{i-1} d\theta_{i+1} ... d\theta_n. \tag{3.2}$$

Since we are only interested in studying the effect of different hadronic inputs in the calculations, and not to assess the degree of dependency of our results on the choice of priors, we have adopted "log" priors in $m_0, m_{1/2}$ and a "flat" prior on A_0 and $\tan\beta$. The reason is

that the soft breaking masses can take any value between, say, the electro-weak scale and a few TeV (to avoid fine-tunning) with the same a priori weight. This is achieved assuming a flat prior on the log of those parameters. For a discussion on the dependency of Bayesian model parameter scans on the choice of prior see for example [24]. The ranges scanned for the cMSSM parameters are 50 MeV $\leq m_0, m_{1/2} \leq 8$ TeV, -7 TeV $\leq A_0 \leq 7$ TeV and $2 \leq \tan\beta \leq 62$ [1]

In addition to the cMSSM model parameters, we include three categories of nuisance parameters in the analysis. Those accounting for the uncertainties on measurements in some of the Standard Model parameters which have been shown to have an important impact in inferences of SUSY models [25], and those from astrophysics and nuclear physics which enter at the level of dark matter direct and indirect detection constraints. As astrophysical nuisance parameters we consider the local dark matter density $\rho_{\rm loc}$, and two quantities parameterizing the local WIMP velocity distribution: the velocity of the Sun in the Galaxy, $v_\odot$, and the velocity dispersion of WIMPs in the halo,v_d, assumed Maxwellian [26]. For the hadronic nuisances we include the hadronic nucleon matrix elements for both spin-independent (f_{Tu}, f_{Td} and f_{Ts}) and spin-dependent (Δ_u, Δ_d and Δ_s) WIMP–nucleon cross sections. For them we adopt informative Gaussian priors as mentioned in Section 2. Table 1 summarizes the values used for the different nuisance parameters considered.

3.1 Experimental constraints

The likelihood function is composed of several different parts, corresponding to the different experimental constraints that are applied in our analysis:

$$\ln\mathcal{L} = \ln\mathcal{L}_{\rm LHC} + \ln\mathcal{L}_{\rm Planck} + \ln\mathcal{L}_{\rm EW} + \ln\mathcal{L}_{\rm B(D)} + \ln\mathcal{L}_{g-2} + \ln\mathcal{L}_{\rm Xe100} + \ln\mathcal{L}_{\rm IC86}. \quad (3.3)$$

The LHC likelihood implements recent null results from SUSY searches from ATLAS. Exclusion limits in the (m_0,$m_{1/2}$) plane are based on a search by the ATLAS collaboration for squarks and gluinos in final states that contain missing E_T, jets and 0 leptons in 5.8 fb $^{-1}$ integrated luminosity of data at $\sqrt{s} = 8$ TeV collision energy [31]. The LHC exclusion limit is included in the likelihood function by defining the likelihood of samples corresponding to masses below the limit to be zero. We furthermore include the most recent experimental constraint from the CMS and ATLAS collaborations on the mass of the lightest Higgs boson which combination is $m_h = 125.66 \pm 0.41$ GeV [32]. We use a Gaussian likelihood and we add in quadrature a theoretical error of 2 GeV to the experimental error. We also include the new LHCb constraint on $BR(\overline{B}_s \to \mu^+\mu^-) = (3.2^{+1.5}_{-1.2}) \times 10^{-9}$, derived from a combined analysis of 1 fb^{-1} data at $\sqrt{s} = 7$ TeV collision energy and 1.1 fb^{-1} data at $\sqrt{s} = 8$ TeV collision energy [33]. We implement this constraint as a Gaussian distribution with a conservative experimental error of $\sigma = 1.5 \times 10^{-9}$, and a 10% theoretical error.

The constraint from the dark matter relic abundance is included as a Gaussian in $\ln\mathcal{L}_{\rm Planck}$. We use the recent PLANCK value $\Omega_\chi h^2 = 0.1196 \pm 0.0031$ [34] and we add a fixed 10% theoretical uncertainty in quadrature. We assume that neutralinos make up all of the dark matter in the universe.

$\ln\mathcal{L}_{\rm EW}$ implements precision tests of the electroweak sector. The electroweak precision observables M_W and $\sin^2\theta_{eff}$ are included with a Gaussian likelihood.

[1] Our motivation for this choice is based on the naturalness criterium which is connected to the fact that SUSY masses above a few TeV lead to a large fine-tunning to reproduce the electro-weak scale. In this respect we are conservative.

Nuisance parameters			
Standard Model			
M_t [GeV]	173.1 ± 1.3		[27]
$m_b(m_b)^{\bar{M}S}$ [GeV]	4.20 ± 0.07		[27]
$[\alpha_{em}(M_Z)^{\bar{M}S}]^{-1}$	127.955 ± 0.030		[27]
$\alpha_s(M_Z)^{\bar{M}S}$	0.1176 ± 0.0020		[28]
Astrophysical			
$\rho_{\rm loc}$ [GeV/cm^3]	0.4 ± 0.1		[29]
$v_\odot$ [km/s]	230.0 ± 30.0		[29]
v_d [km/s]	282.0 ± 37.0		[29]
Hadronic			
	LQCD	Experiment	
f_{Tu}	0.0190 ± 0.0029	0.0308 ± 0.0061	[30], [19]
f_{Td}	0.0246 ± 0.0037	0.0459 ± 0.0089	[30], [19]
f_{Ts}	0.043 ± 0.011	0.493 ± 0.159	[17], [19]
Δ_u	0.787 ± 0.158	0.75 ± 0.05	[13], [21]
Δ_d	-0.319 ± 0.066	-0.34 ± 0.07	[13], [21]
Δ_s	-0.020 ± 0.011	-0.09 ± 0.02	[13], [22]

Table 1. Nuisance parameters adopted in the scans of the cMSSM parameter space, indicating the mean and standard deviation used for the Gaussian prior on each of them. The matrix elements f_{Tu} and f_{Td} are extracted from the value of $\sigma_{\pi N}$ following [9]. We use values of $\sigma_{\pi N}$ derived from LQCD calculations ($\sigma_{\pi N}$=43±6.1 MeV [30]) and derived from the mass spectrum of exotic baryons ($\sigma_{\pi N}$=74±12 MeV [19]) as two extreme representative values of the range of $\sigma_{\pi N}$ found in the literature. For the LQCD value of f_{Ts} we use the most recent world average from LQCD calculations, $\sigma_{\pi N}$=40±10 MeV [17].

Relevant constraints from B and D physics are included in $\ln \mathcal{L}_{\rm B(D)}$ as a Gaussian likelihood. The full list of B and D physics observables included in our analysis is shown in table 2.

The measured anomalous magnetic moment of the muon, included as a Gaussian datum in $\ln \mathcal{L}_{g-2}$, provides important information about the supersymmetric parameter space, since it can be experimentally measured to very good precision. By comparing the theoretical value of this quantity favored in the Standard Model with the experimental result the supersymmetric contribution δa_μ^{SUSY} can be constrained. The experimental measurement of the muon anomalous magnetic moment based on e^+e^- data is in tension with the Standard Model prediction by $\delta a_\mu^{SUSY} = (28.7 \pm 8.0) \times 10^{-9}$ [35], i.e., a 3.6σ discrepancy between the experimental result and the expected value from Standard Model physics alone.

As for constraints from direct dark matter search experiments we use the recent results from XENON100 with 225 live days of data collected between February 2011 and March 2012 with 34 kg fiducial volume [36]. We calculate the number of expected signal recoil events from each of the points on our scan as

$$N_s^{XE}(\mathbf{\Theta}) = T \frac{\rho_{\rm loc}}{m_\chi} \frac{M}{m_A} \cdot \int_{E_{\rm thr}} dE \int_{v<v_{\rm esc}} d{\rm v}\, v f({\rm v} + {\rm v}_{\rm Earth}) \frac{d\sigma_{\chi N}(\mathbf{\Theta}, v, E)}{dE} \,, \qquad (3.4)$$

where T and M are the exposure of and total mass of the detector respectively, m_A is the detector nucleus target mass, $\rho_{\rm loc}$ is the local dark matter density, v the dark matter velocity in the detector rest frame, $\rm v_{Earth}$ the Earth velocity in the rest frame of the Galaxy, $f(.)$

the dark matter velocity distribution function (assumed Maxwellian) and $d\sigma_{\chi N}/dE$ is the differential cross section for the interaction between the neutralino and the nucleus. The integral is over the volume of phase space for which v is smaller than the escape velocity $v_{\rm esc}$ and larger than the minimal velocity $v_{\rm min}(E)$ able to produce a recoil with energy E, above the detector energy threshold, $E_{\rm thr}$. We follow the treatment of XENON100 data as described in detail in [4], building the likelihood function, $\ln \mathcal{L}_{\rm Xe100}$, as a Poisson distribution for observing N recoil events when $N_s(\mathbf{\Theta})$ signal plus N_b background events are expected. The expected number of events from the background-only hypothesis in the XENON100 run is $N_b = 1.0 \pm 0.2$, while the collaboration reported N=2 events observed in the pre-defined signal region. We use the latest values for the fiducial mass and exposure time of the detector, and we include the reduction of the lower energy threshold for the analysis to 3 photoelectron events and an update to the response to 122 keV gamma-rays to 2.28 PE/keVee, obtained from new calibration measurements, in accordance with the values reported in Ref. [36]. We make the simplifying assumption of an energy-independent acceptance of data quality cuts, and adjust the acceptance-corrected exposure to accurately reproduce the exclusion limit in the $(m_{\tilde{\chi}_1^0}, \sigma^{\rm SI}_{\chi N})$ plane reported in Ref. [36] in the mass range of interest.

In a similar fashion, the likelihood of IceCube, $\ln \mathcal{L}_{\rm IC86}$, is based on the number of signal events expected,

$$N_s^{IC}(\mathbf{\Theta}) \;=\; T \cdot \int_{E_{thr}} \frac{dN_\nu(\mathbf{\Theta})}{dt dE_\nu dA}\, A_{eff}(E_\nu)\, dE_\nu \,, \tag{3.5}$$

where T is the exposure time, A_{eff} is the detector effective area, E_{thr} is the energy threshold of the detector and $dN_\nu/dE_\nu dA$ is the differential muon–neutrino flux at the Earth from WIMP annihilation for a given choice of cMSSM parameters. The effective area is a measure of the efficiency of the detector to the signal, and includes the neutrino-nucleon interaction probability, the energy loss of the produced muon from the interaction point to the detector and the detector trigger and analysis efficiency. We use the public information about the 86-string configuration of IceCube released with DarkSUSY, ie, the estimated effective area of the detector and the background pdf. IceCube has reported no signal on their searches for an excess neutrino flux from the Sun in their analysis with the 79-string configuration [37], so we assume here a background–only scenario. We build the Likelihood for IceCube following [38]: given a number of signal events for a given model and the number of estimated background events obtained by sampling the background pdf, we use a Poisson likelihood convoluted with a log-normal distribution for the uncertainty on the estimation of the number of signal events. This uncertainty takes into account the uncertainty in the effective area and in the signal prediction for which we use a 10% relative error for this quantity. We further use an angular cut of $\phi_{cut} = 10^{\rm o}$ around the solar position. We normalize our results to one calendar year of IceCube data taking. We assume no contamination in the background estimation from remaining misreconstructed atmospheric muons. We have neglected the potential contribution to the background from cosmic ray interactions in the Sun corona. This flux has been estimated in [39] and predicts about 1 event per year in IceCube. We have also neglected the effects arising from uncertainties in the Solar composition [40] and in the capture rate from other planets, which has been shown to be negligible [41].

3.2 Scanning technique

The full list of experimental constraints included in the likelihood function is given in Table 2. In order to explore the posterior pdf we use the `SuperBayeS-v2.0` package [49]. This latest version of `SuperBayeS` is interfaced with SoftSUSY 3.2.7 as SUSY spectrum calculator,

Observable	Mean value	Uncertainties		Ref.
	μ	σ (exper.)	τ (theor.)	
M_W [GeV]	80.399	0.023	0.015	[42]
$\sin^2\theta_{eff}$	0.23153	0.00016	0.00015	[42]
$\delta a_\mu^{\rm SUSY} \times 10^{10}$	28.7	8.0	2.0	[35]
$BR(\overline{B} \to X_s\gamma) \times 10^4$	3.55	0.26	0.30	[43]
$R_{\Delta M_{B_s}}$	1.04	0.11	-	[44]
$\frac{BR(B_u\to\tau\nu)}{BR(B_u\to\tau\nu)_{SM}}$	1.63	0.54	-	[43]
$\Delta_{0-} \times 10^2$	3.1	2.3	-	[45]
$\frac{BR(B\to D\tau\nu)}{BR(B\to De\nu)} \times 10^2$	41.6	12.8	3.5	[46]
R_{l23}	0.999	0.007	-	[47]
$BR(D_s \to \tau\nu) \times 10^2$	5.38	0.32	0.2	[43]
$BR(D_s \to \mu\nu) \times 10^3$	5.81	0.43	0.2	[43]
$BR(D \to \mu\nu) \times 10^4$	3.82	0.33	0.2	[43]
$\Omega_\chi h^2$	0.1196	0.0031	0.012	[34]
m_h [GeV]	125.66	0.41	2.0	[32]
$BR(\overline{B}_s \to \mu^+\mu^-)$	3.2×10^{-9}	1.5×10^{-9}	10%	[33]
	Limit (95% CL)		τ (theor.)	Ref.
Sparticle masses	As in Table 4 of Ref. [48].			
$m_0, m_{1/2}$	ATLAS, $\sqrt{s} = 8$ TeV, 5.8 fb^{-1}2012 limits			[31]
$m_\chi - \sigma_{\chi N}^{\rm SI}$	XENON100 2012 limits (224.6 × 34 kg days)			[36]

Table 2. Summary of the observables used for the computation of the likelihood function For each quantity we use a likelihood function with mean μ and standard deviation $s = \sqrt{\sigma^2 + \tau^2}$, where σ is the experimental uncertainty and τ represents our estimate of the theoretical uncertainty. Lower part: Observables for which only limits currently exist. The explicit form of the likelihood function is given in ref. [48], including in particular a smearing out of experimental errors and limits to include an appropriate theoretical uncertainty in the observables.

MicrOMEGAs 2.4 [50] to compute the abundance of dark matter, DarkSUSY 5.0.5 [26] for the computation of $\sigma_{\chi N}^{\rm SI}$ and $\sigma_{\chi N}^{\rm SD}$, SuperIso 3.0 [51] to compute $\delta a_\mu^{\rm SUSY}$ and B(D) physics observables, SusyBSG 1.5 for the determination of $BR(\overline{B} \to X_s\gamma)$ [52].

The `SuperBayeS-v2.0` package uses the publicly available MultiNest v2.18 [53, 54] nested sampling algorithm to explore the cMSSM model parameter space. MultiNest has been developed in such a way as to be an extremely efficient sampler even for likelihood functions defined over a parameter space of large dimensionality with a very complex structure as it is the case of the cMSSM. The main purpose of the Multinest is the computation of the Bayesian evidence and its uncertainty but it produces posterior inferences as a by–product. Besides it is also able to reliably evaluate the profile likelihood, given appropriate MultiNest settings, as demonstrated in [55].

4 Results

In this section we present the results of the different scans we performed and comment on the conclusions that can be extracted on the effect of using LQCD or the experimental determination of the nucleon matrix elements in interpreting experimental results.

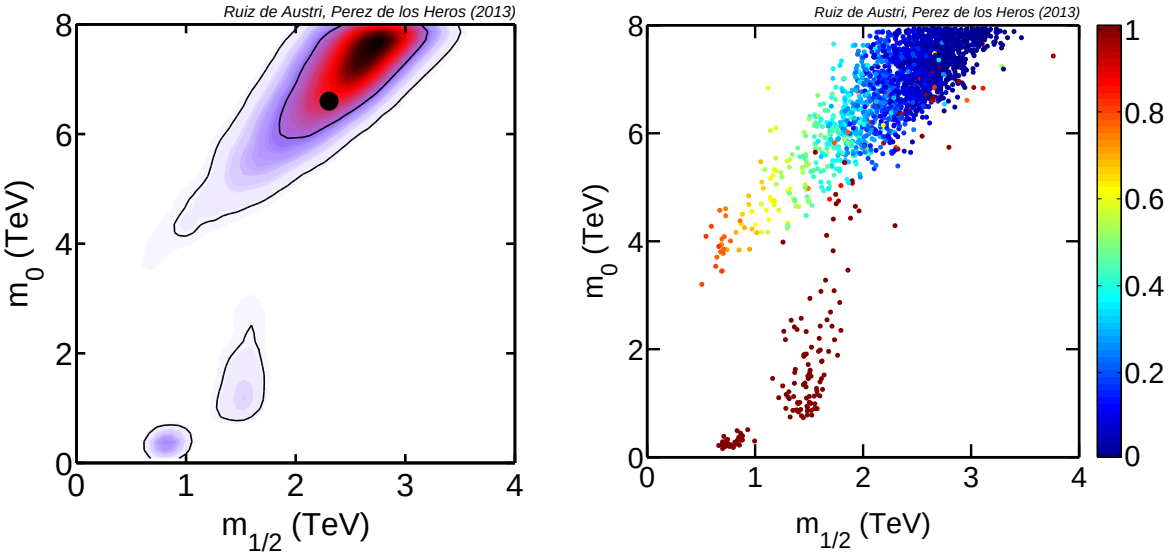

Figure 1. **Left:** 2D marginalized posterior pdf of the ($m_{1/2}$,m_0) plane from the cMSSM scan including particle physics and cosmological constraints from table 2, excepting dark matter detection constraints. The inner and outer contours enclose respective 68% and 95% joint regions. The filled circle indicates the posterior mean. **Right:** As in the left plot but showing the composition of the neutralino as gaugino fraction in the color scale. The density of samples reflects the probability density.

4.1 Results with no dark matter detection data

We begin by showing in Fig. 1 the impact of the current experimental constraints on the cMSSM from the inputs shown in table 2, not including XENON100 and IceCube data. The results are shown in the ($m_{1/2}$,m_0) plane. The left panel displays the marginalized posterior pdf including the 68%, 95% credible intervals whilst the right panel shows the gaugino fraction of the neutralino.

Most of the posterior pdf lies in the high-mass region due to the Higgs mass measurement reported by ATLAS and CMS. The reason is that large radiative corrections are needed to reconciliate theory and experiment and this can be achieved either with stops masses $\gtrsim 3$ TeV and non-small $tan\beta$ to enhance the logarithmic corrections or/and through the maximal mixing scenario where the stop mixing parameter $X_t = A_t - \mu \cot\beta$ satisfies $X_t = \pm\sqrt{6} M_{SUSY}$ being M_{SUSY} a certain average of the stop masses. Whereas the later condition implies a certain degree of fine-tunning, the former is easy to accommodate requiring large soft-mases [56]. Therefore it is expected that large gaugino and scalar masses are statistically favored. This region corresponds to the so called Focus-Point region [57] where scalar masses are multi-TeV while there is not much fine-tunning, thus, preserving the naturalness criterion [2] and where the neutralino is a Higgsino or a mixture of Higgsino-bino. It is precisely the Higgsino fraction which makes its self-annihilation very efficient to gauge bosons and top quarks. Besides, it coannihilates with the lightest charginos and the second lightest neutralino. Actually for low or intermediate masses the annihilation is so efficient that its relic density can be below the measured dark matter relic density. Thus, it needs a

[2]The authors of [58–60] have shown how the fine-tunning penalization arises naturally in the Bayesian framework.

sizable bino fraction to be a viable dark matter candidate. As long as the gaugino mass increases, the neutralino gets a larger Higgsino fraction until becoming pure Higgsino. In this limit, the largest acceptable mass is $m_{\tilde{\chi}_1^0} \simeq 1$ TeV [61]. This is verified in the right panel of Figure 1, which shows the gaugino fraction of the neutralino, g_f. This fraction is defined as $g_f = |N_{11}|^2 + |N_{12}|^2$, where the N_{1i} represent the bino and wino component of the lightest neutralino respectively. The other regions of the cMSSM where the required dark matter density is reproduced, namely, the stau-coannihilation region where the neutralino LSP coannihilates with the lightest stau, and the A-funnel region where $2m_{\tilde{\chi}_1^0} \simeq m_A$ and the annihilation goes via a resonance process to pairs of fermions appear at the 95% credible level and are statistically disfavored relatively to the Focus-Point region as they correspond to rather small soft-masses.

Since quite high supersymmetric masses are favored, the supersymmetric effects on g-2 and B-physics observables are negligible, thus, their role in the analysis is diluted.

Fig. 2, shows the posterior pdfs in the $(m_{\tilde{\chi}_1^0}, \sigma^{\rm SI}_{\chi N})$ plane (upper panels) and in the $(m_{\tilde{\chi}_1^0}, \sigma^{\rm SD}_{\chi N})$ plane (lower panels). The left panels use the LQCD estimation of the nucleon matrix elements, whereas the right ones the experimental measurement assuming that $\sigma_{\pi N} = 74$ MeV as outlined in Section 1.

Following the discussion above, it is clear that the bulk of the posterior pdf lies in the Focus-Point region which covers neutralino masses from a few hundred GeV to ~ 1 TeV. In this region the spin-independent cross section, shown in the top panels, is large because the neutralino is a mixed bino-Higgsino state and the dominant diagrams entering in the process are mediated by a Higgs H/h which scale as $\propto |N_{11}|^2 |N_{14/13}|^2$, where $N_{14/13}$ represent the Higgsino composition of the lightest neutralino. As long as the gaugino mass increases the neutralino eventually becomes a pure Higgsino and the sensitivity is lost. In the stau-coannihilation and the A-funnel regions, the neutralino is bino-like and therefore the spin-independent cross section is suppressed. The A-funnel region has a larger spin-independent cross section because $tan\beta$ is typically larger and the heavy Higgs contribution is enhanced with respect to the one in the stau-coannihilation region.

The effect of using different determinations of the nucleon matrix elements in the spin-independent cross section is dramatic, as can be seen by comparing the left and right top panels. The posterior pdf is shifted by almost a factor 10 due to the large differences in the estimation of the strangeness content of the nucleon f_{T_s} , which is the dominant contribution in the evaluation of the spin-independent cross section, between LQCD and the experimental approaches. This is precisely the difference since f_{T_s} acts as a proportionality factor in the coupling of the neutralino to the nucleon, as shown in Eq. 2.1. Therefore it is expected that results from XENON100 on the spin-independent cross section disfavors a larger portion of the Focus-Point when using the experimental values of f_{T_s}, thus having a bigger impact on the ($m_{1/2}$,m_0) plane. We will come back to this point later.

Let us now discuss the spin-dependent cross section which is shown in the lower panels of Fig. 2. Due to the LHC bounds on squark masses which currently are constrained to be above ~ 1 TeV, this is largely governed by Z-boson exchange and is sensitive to the Higgsino asymmetry $\sigma^{\rm SD}_{\chi N} \propto (|N_{13}|^2 - |N_{14}|^2)^2$ since the bino is a SU(2) singlet and it does not couple to the Z-boson. Therefore the spin-dependent cross section is significantly increased in the mixed bino-Higgsino neutralino scenario while being suppressed for a pure Higgsino-like neutralino. This is precisely what is shown in the plots.

Comparing the upper and lower panels one can see that in contrast to the spin-independent counterpart, the spin-dependent cross section is remarkably stable to the choice of the nu-

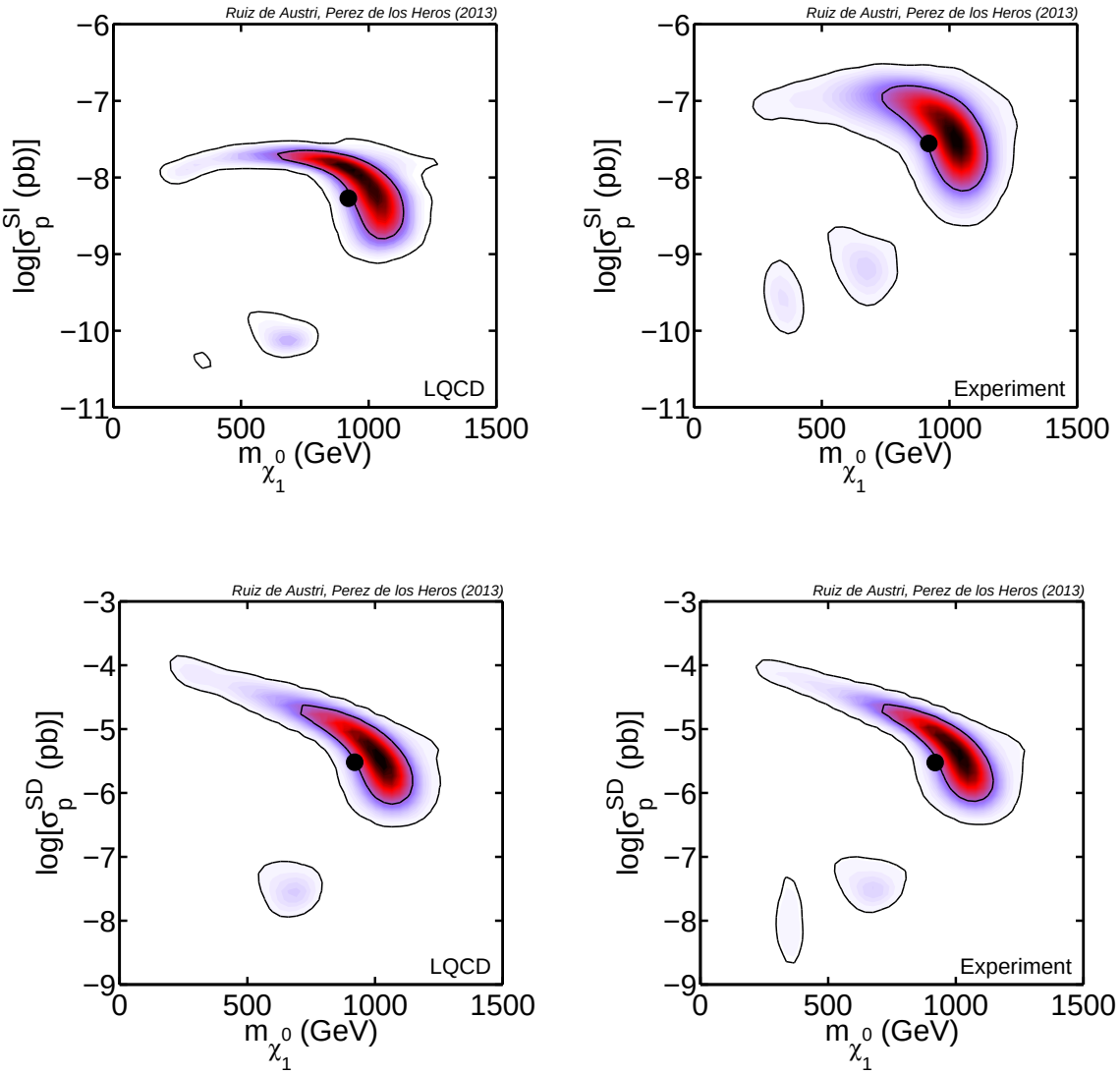

Figure 2. **Upper panel:** 2D marginalized posterior pdfs of the $(m_{\tilde{\chi}_1^0}, \sigma_{\chi N}^{\rm SI})$ plane obtained using the values of the hadronic structure functions from LQCD (left) and experimental calculations (right) with all the particle physics and cosmological constraints in table 2 included, excepting dark matter detection constraints. **Lower panel:** Same as above but for the $(m_{\tilde{\chi}_1^0}, \sigma_{\chi N}^{\rm SD})$ plane.

cleon matrix elements type of determination. This is because, for the latter, the dominant contribution of the nucleon matrix elements come from the up/down quark flavors which are consistent at the 1-σ level within LQCD and the experimental approaches.

4.2 Results including dark matter direct detection data

Next, we focus on the impact of XENON100 data on the cMSSM which we show in Fig. 3. The upper panels show the $(m_{1/2}, m_0)$ plane when limits from XENON100 are included.

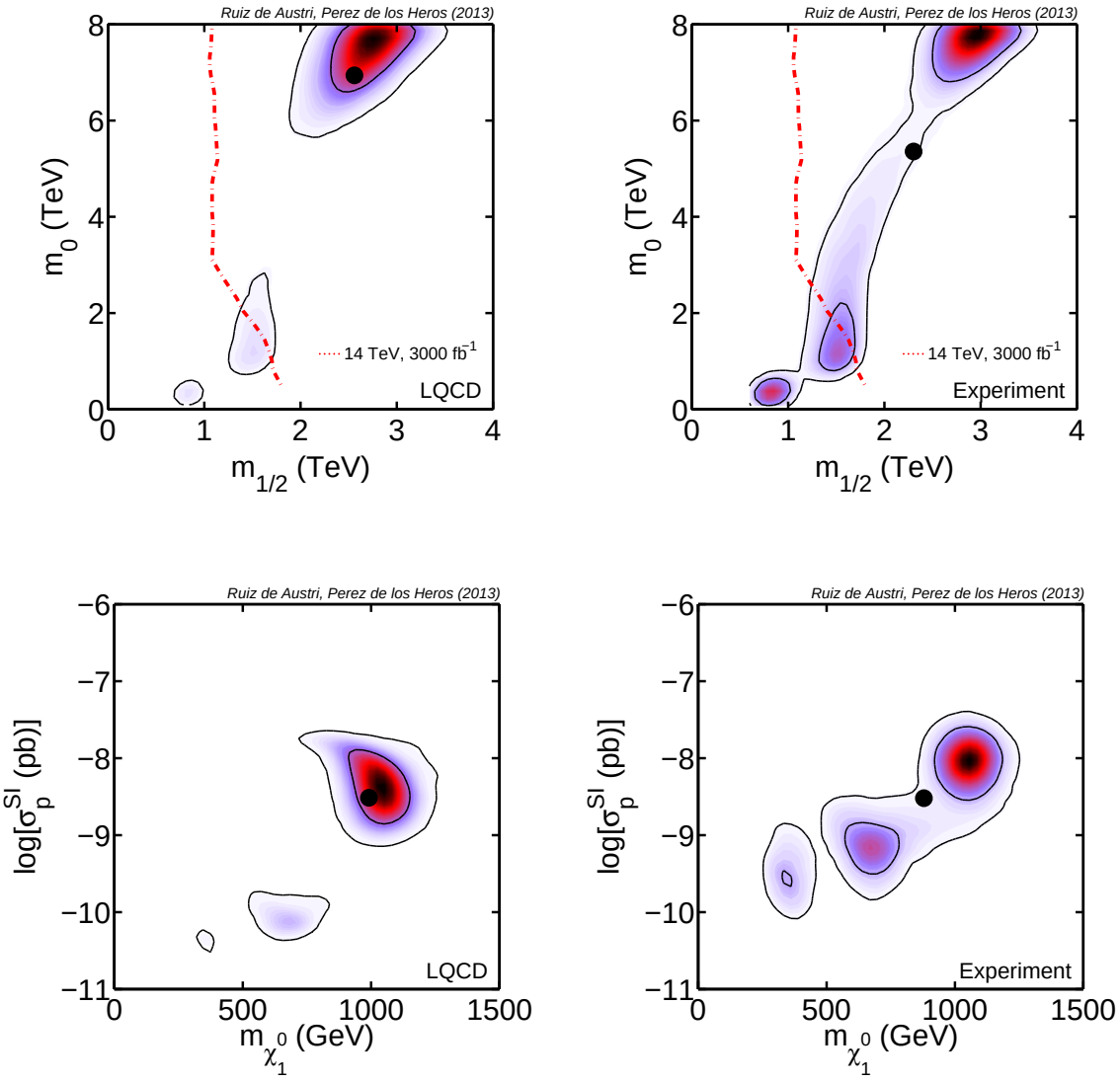

Figure 3. **Upper panel:** 2D marginalized posterior pdfs of the ($m_{1/2}$,m_0) plane from the cMSSM scan including particle physics and cosmological constraints from table 2 as well as XENON100 constraints, obtained using the values of the hadronic structure functions from LQCD (left) and experimental calculations (right). The dot-dashed/red line shows the projected ultimate LHC reach in the high-luminosity phase with an energy of 14 TeV and an integrated luminosity of 3000 fb^{-1} (from [62]). **Lower panel:** Same as above but for the ($m_{\tilde{\chi}_1^0}, \sigma^{\rm SI}_{\chi N}$) plane.

The lower panels show the ($m_{\tilde{\chi}_1^0}, \sigma^{\rm SI}_{\chi N}$) plane. Left panels use the LQCD determination of the nucleon matrix elements whereas the right ones the experimental one. Clearly XENON100 data disfavors the Focus-Point region, as expected from the discussion above, since the neutralinos are mixed bino-Higgsinos with masses of $\mathcal{O}$(100 GeV). The role of the XENON100 data on the ($m_{1/2}$, m_0) plane changes dramatically when either the LQCD or the experimental approaches are used to extract the strangeness content of the nucleon. In the latter

case a larger portion of the Focus-Point region is disfavored and therefore a sizable fraction of the posterior pdf is displaced to the stau-coannihilation and A-funnel regions which now are favored at the 68 % credible level.

As an example, we display the projected ultimate LHC reach in the high-luminosity phase with an energy of 14 TeV and an integrated luminosity of 3000 fb^{-1} [62]. One can conclude that, regarding LHC searches, there are much better detection prospects in the case of assuming higher values of the f_T coefficients, represented by the experimentally obtained values in our study.

The $(m_{\tilde{\chi}_1^0}, \sigma_{\chi N}^{\rm SI})$ plane shows that XENON100 data have a significant softer impact when LQCD nucleon form factors are employed. In this case (left-panel) neutralinos of the bino-Higgsinos mix type are still favored in the Focus-Point region at the 95 % credible level, whereas when applying experimental data, in essence, only the pure Higgsino scenario remains in the Focus-Point region. The connected bimodal type of shape shown by the posterior pdf is an effect of the mentioned displacement of the posterior towards the A-funnel funnel region where lower spin-independent cross sections are favored. The remaining probability island which exists at the 68 % credible level corresponds to the stau-coannihilation region.

4.3 Results including dark matter indirect detection data

Fig. 4 shows the impact of IceCube86 data only (i.e. non including XENON100 data) in the $(m_{1/2}, m_0)$ plane on the upper panels and $(m_{\tilde{\chi}_1^0}, \sigma_{\chi N}^{\rm SD})$ on the lower panels.

As pointed out previously, the spin-independent and spin-dependent cross sections are correlated through the Higgsino fraction of the neutralino. Actually as long as the Higssino fraction is larger than $\mathcal{O}(10\%)$, cross sections which are at reach to both XENON100 and IceCubeC86 can be achieved. Therefore one expects that the Focus-Point region be also probed by IceCube86 as it is done by XENON100. This is what can be observed in the upper panels of Fig. 4. Of course, in points where the neutralino becomes Higgsino dominated, the spin-dependent cross section drops and the sensitivity is lost. In comparison with the SI counterpart, the posterior pdf is remarkably stable to the choice of the method to determine the nucleon matrix elements as argued above (only a small fraction of the posterior pdf is displaced to both the A-funnel and stau-coannihilation regions that now remain disconnected though). Therefore the bulk of the posterior pdf lies well in the Focus-Point for both choices. In this case one can conclude that the chance to probe the model at the LHC is small in either approach.

The lower panels of Fig. 4 show the same behavior: the allowed region in the $(m_{\tilde{\chi}_1^0}, \sigma_{\chi N}^{\rm SD})$ plane hardly changes in the two scenarios considered. The 68 % credible level which corresponds to Higgsino-like neutralinos is qualitatively similar between the LQCD and the experimental approaches, and just the tails differ, allowing lighter neutralinos in the former case, with cross sections above $\sim 10^{-6}$ pb.

5 Conclusions

In this work we have investigated the impact of using different values of the nucleon matrix elements in inferences of the cMSSM parameter space, though the conclusions can be extrapolated qualitatively to any other SUSY model without loosing generality. Among the wide range of values of the nucleon matrix elements found in the literature obtained by different groups, we have chosen typical extreme values of the range to illustrate the impact they can have on the interpretation of dark matter searches. We have used estimations from recent

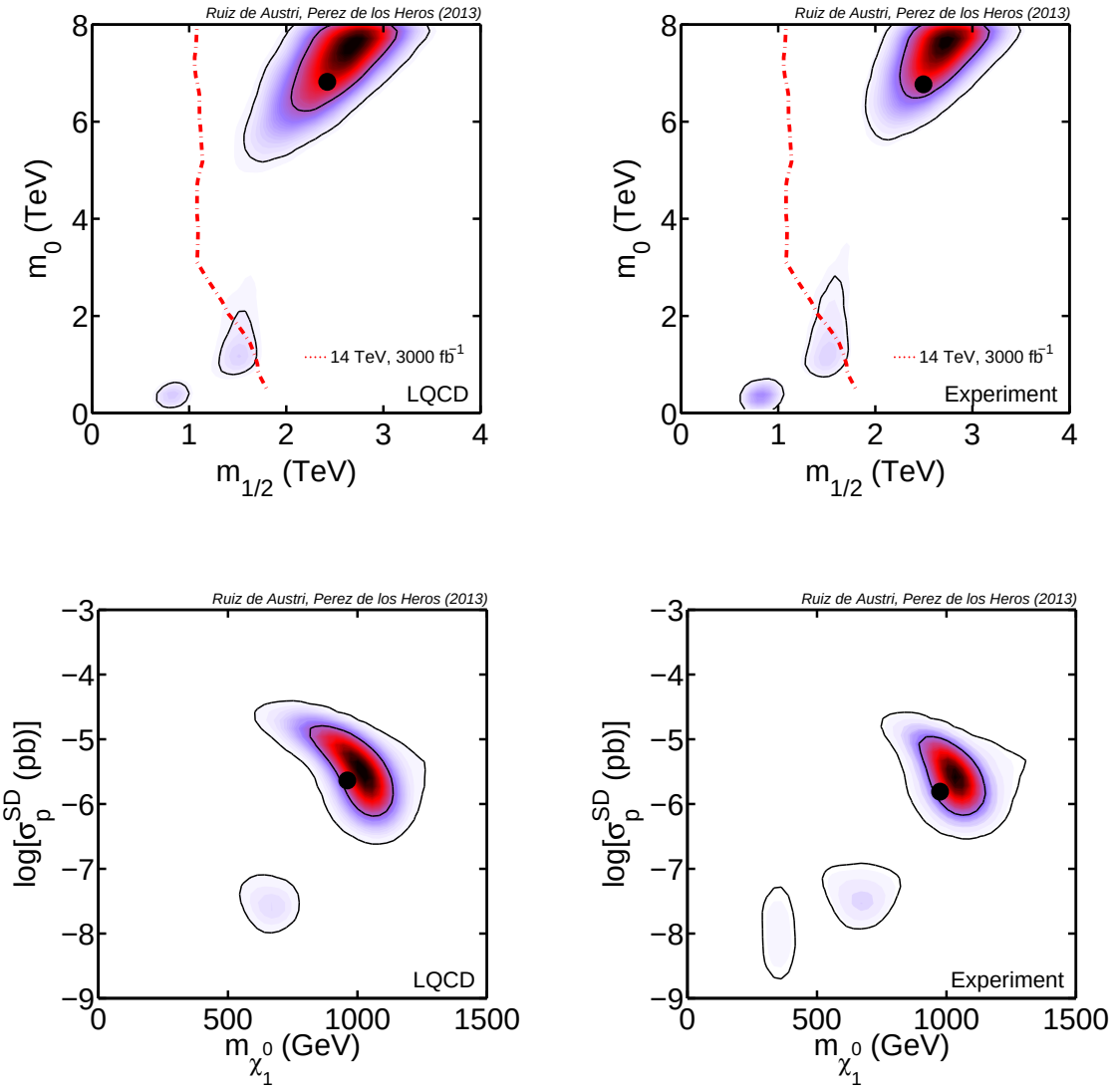

Figure 4. **Upper panel:** 2D marginalized posterior pdfs of the ($m_{1/2}$,m_0) plane from the cMSSM scan including particle physics and cosmological constraints from table 2 and IceCube86 constrains, but excepting XENON100 constraints, obtained using the values of the hadronic structure functions from LQCD (left) and experimental calculations (right). The dot-dashed/red line shows the projected ultimate LHC reach in the high-luminosity phase with an energy of 14 TeV and an integrated luminosity of 3000 fb^{-1} (from [62]). **Lower panel:** Same as above but for the ($m_{\tilde{\chi}_1^0}, \sigma^{\rm SD}_{\chi N}$) plane.

LQCD calculations as well as experimental results, using these different values of the nucleon matrix elements as inputs to different scans over the cMSSM parameter space.

We have shown that the role of dark matter experiments sensitive to spin-independent cross sections, like XENON100, is strongly affected by the large differences in the determination of the strangeness content of the nucleon. The reason is that spin-independent cross sections can vary up a factor ~ 10 depending on which input for the nucleon matrix elements

is used. The posterior pdf of a given model is displaced rougly by that factor. The immediate result is that a larger portion of the Focus-Point region is disfavored by current direct dark matter searches when using nucleon data that favor a larger strangeness content of the nucleon. Note that the most disfavored regions from the Higgs mass constraint from the LHC (not including XENON100 data), as the stau-coannihilation and A-funnel regions, get a high statistical weight when using a high value of the nucleon matrix elements, represented in our study by the experimental value. This has a strong impact for the interpretation of SUSY searches at the LHC. The accessible region of parameter space changes radically whether low or high values of the matrix elements are used. However, if future ton-scale direct dark matter experiments can probe, as expected, spin-independent cross section levels of about 10^{-11} pb, the dependence on the matrix elements will be alleviated, since at that level that dependence becomes negligible and, at least in the case of the cMSSM, practically all the currently allowed parameter space can be probed.

The conclusion is more favorable for experiments sensitive to the spin-dependent cross section, like neutrino telescopes. They are practically not affected by the choice of values of the nuclear axial-vector matrix elements which drive the spin-dependent neutralino-nucleon cross section. The reason is that even if there is a large difference in the strangeness content of the nucleon for spin-dependent interactions, light quarks play here a prominent role, and the determination of their content in the nucleon from LQCD calculations or experimental results is consistent at 1-σ level. To illustrate this we have applied constraints from IceCube in our cMSSM scans assuming a background–only scenario with the 86 strings configuration, inspired by their recent null result on searches for an excess muon flux from neutralino annihilations in the Sun. In view of the results shown in Fig. 4 it can be stated that current limits from neutrino telescopes on the spin-dependent neutralino-nucleon cross section are robust in what concerns the choice of nucleon matrix elements, and these quantities should not be a concern in interpreting neutrino telescope results.

Acknowledgments

We thank the Kavli Institute for Theoretical Physics at UCSB and organizers of the Hunting for Dark Matter programme for their hospitality during the preparation of this manuscript. This research was supported in part by the National Science Foundation under Grant No. NSF PHY11-25915. R. RdA, is supported by the Ramón y Cajal program of the Spanish MICINN and also thanks the support of the Spanish MICINN's Consolider-Ingenio 2010 Programme under the grant MULTIDARK CSD2209-00064 and the Invisibles European ITN project (FP7-PEOPLE-2011-ITN, PITN-GA-2011-289442-INVISIBLES). The use of IFT-UAM High Performance Computing Service is gratefully acknowledged.

References

[1] G. Bertone, D. G. Cerdeño, M. Fornasa, R. Ruiz de Austri, C. Strege and R. Trotta, JCAP **1201** (2012) 015.

[2] C. Strege, G. Bertone, D. G. Cerdeño, M. Fornasa, R. Ruiz de Austri and R. Trotta, JCAP **1203** (2012) 030.

[3] O. Buchmueller, R. Cavanaugh, M. Citron, A. De Roeck, M. J. Dolan, J. R. Ellis, H. Flacher and S. Heinemeyer *et al.*, Eur. Phys. J. C **72** (2012) 2243.

[4] C. Strege, G. Bertone, F. Feroz, M. Fornasa, R. Ruiz de Austri and R. Trotta, JCAP **1304** (2013) 013.

[5] A. Fowlie, K. Kowalska, L. Roszkowski, E. M. Sessolo and Y. -L. S. Tsai, arXiv:1306.1567 [hep-ph].

[6] G. Jungman, M. Kamionkowski and K. Griest, *Phys. Rept.* **267** (1996) 195.

[7] A. Bottino, F. Donato, N. Fornengo and S. Scopel, Astropart. Phys. **13** (2000) 215.

[8] A. Bottino, F. Donato, N. Fornengo and S. Scopel, Astropart. Phys. **18** (2002) 205.

[9] J. Ellis K. Olive and C. Savage, *Phys. Rev. D* **77** (2008) 065026.

[10] C. Arina, G. Bertone and H. Silverwood, *Phys. Rev. D* **88** (2013) 013002.

[11] J. Engel, S. Pittel and P. Vogel, *Int. J. Mod. Phys. E* **1** (1992) 1.

[12] R D. Young and A. W. Thomas. Proc. 4th Intl. Symposium on Symmetries in Subatomic Physics (SSP2009), Taipei, Taiwan, June 2-5 2009, arXiv:0911.1757.

[13] G. S. Bali *et al.* , *Phys. Rev. Lett.* **108** (2012) 222001.

[14] D. G. Cerdeño, M. Fornasa, J.-H. Huh and M. Peiró, *Phys. Rev. D* **87**, (2013) 023512.

[15] R. Trotta, R. Ruiz de Austri and C. Pérez de los Heros *JCAP* **0908** (2009) 034.

[16] G. L. Kane, C. F. Kolda, L. Roszkowski and J. D. Wells, *Phys. Rev. D* **49** (1994) 6173.

[17] P. Junnarkar and A. Walker-Loud, arXiv:1301.1114.

[18] J. Stahov, H. Clement and G. J. Wagner, arXiv:1211.1148.

[19] P. Schweitzer *Eur. Phys. J.* A**22** (2004) 89.

[20] M. M. Pavan, I. I. Strakovsky, R. L. Workman and R. A. Arndt. *PiN Newslett.* 16 (2002) 110. [arXiv:hep-ph/0111066]

[21] M. Alekseev *et al.* , *Phys. Lett. B***693** (2010) 227.

[22] M. Alekseev *et al.* , *Phys. Lett. B***660** (2008) 458.

[23] C. A. Aidala, S. D. Bass, D. Hasch and G. K. Mallot, arXiv:1209.2803.

[24] R. Trotta, F. Feroz, M. P. Hobson, L. Roszkowski and R. Ruiz de Austri, *JHEP* **0812** (2008) 024.

[25] L. Roszkowski, R. Ruiz de Austri and R. Trotta, *JHEP* **0707** (2007) 075.

[26] P. Gondolo *et al.* , *JCAP* **07** (2004) 008.

[27] J. Beringer *et al.* (Particle Data Group), *Phys. Rev. D***86** (2012) 010001.

[28] K. Hagiwara, A. D. Martin, D. Nomura and T. Teubner, *Phys. Lett. B* **649** (2007) 173.

[29] M. Pato *et al.* , *Phys. Rev. D* **83** (2011) 083505.

[30] X.-L. Ren, L. S. Geng, J. Martin Camalich, J. Meng and H. Toki, *J. High Energy Phys.***12** (2012) 073.

[31] ATLAS Collaboration, ATLAS-CONF-2012-109.

[32] http://moriond.in2p3.fr/QCD/2013/MorQCD13Prog.html.

[33] R. Aaij *et al.* , *Phys. Rev. Lett.***110** (2013) 021801.

[34] P. A. R. Ade *et al.* , arXiv:1303.5076.

[35] M. Davier, A. Hoecker, B. Malaescu and Z. Zhang, *Eur. Phys. J. C* **71** (2011) 1515.

[36] E. Aprile *et al.* , *Phys. Rev. Lett.* **109** (2012), 181301.

[37] M. G. Aarsten *et al.* , *Phys. Rev. Lett.* **110** (2013) 131302.

[38] P. Scott *et al.* , *JCAP* **11** (2012) 057.

[39] G. L. Fogli, E. Lisi, A. Mirizzi, D. Montanino and P. D. Serpico, *Phys. Rev. D***74** (2006) 093004.

[40] J. Ellis, K. A. Olive, C. Savage and V. C. Spanos, *Phys. Rev. D***81** (2010) 085004.

[41] S. Sivertsson and J. Edsjö, *Phys. Rev. D***85** (2012) 123514.

[42] `http://lepewwg.web.cern.ch/LEPEWWG`.

[43] D. Asner *et al.* , arXiv:1207.1158 (also arXiv:1010.1589).

[44] R. Aaij *et al. Phys. Lett. B***709** (2012) 177; A. Abulencia *et al. Phys. Rev. Lett.***97** (2006) 242003; CKMfitter Group, http://ckmfitter.in2p3.fr.

[45] Value obtained combining the Babar measurement B. Aubert et al. `arXiv:0808.1915` with the results of K. Nakamura et al. [Particle Data Group], J. Phys. G37, 075021 (2010) and M. Nakao et al. Phys. Rev. D69, 112001 (2004).

[46] B. Aubert *et al.* , Phys. Rev. Lett. **100** (2008) 021801.

[47] M. Antonelli *et al.* , Nucl. Phys. Proc. Suppl. **181-182** (2008) 83.

[48] R. Ruiz de Austri, R. Trotta and L. Roszkowski, *JHEP* **0605** (2006) 002.

[49] Available from `http://superbayes.org`.

[50] G. Belanger *et al.* , *Comput. Phys. Commun.* **182** (2011) 842.

[51] F. Mahmoudi, *Comput. Phys. Commun.* **178** (2008) 745; F. Mahmoudi, *Comput. Phys. Commun.* **180** (2009) 1579.

[52] G. Degrassi, P. Gambino and P. Slavich, Comput. *Phys. Commun.* **179** (2008) 759.

[53] F. Feroz and M. P. Hobson, *Mon. Not. Roy. Astron. Soc.* **384** (2008) 449.

[54] F. Feroz, M. P. Hobson and M. Bridges, *Mon. Not. Roy. Astron. Soc.* **398** (2009) 1601.

[55] F. Feroz, K. Cranmer, M. Hobson, R. Ruiz de Austri and R. Trotta, *JHEP* **1106** (2011) 042.

[56] A. Djouadi, *Phys. Rept.* **459** (2008) 1.

[57] J. L. Feng, K. T. Matchev and T. Moroi, *Phys.Rev.Lett.* **84** (2000) 2322.

[58] M. E. Cabrera, J. A. Casas and R. Ruiz de Austri, JHEP **0903** (2009) 075.

[59] M. E. Cabrera, J. A. Casas and R. Ruiz de Austri, JHEP **1005** (2010) 043.

[60] M. E. Cabrera, J. A. Casas and R. Ruiz de Austri, arXiv:1212.4821.

[61] N. Arkani-Hamed, A. Delgado and G. Giudice, *Nucl.Phys.* **B741** (2006) 108.

[62] **ATLAS** Collaboration, ATL-PHYS-PUB-2012-001, CERN, Geneva, Aug, 2012.